

# Study on the characterization of polarization-controlling photonic nanostructures

Wenbo Lin<sup>1</sup> and Saeko Tachikawa<sup>2</sup>

<sup>1</sup>*Iwamoto group, Department of Electrical Engineering and Information Systems, Graduate School of Engineering, The University of Tokyo*

<sup>2</sup>*Nomura group, Department of Electrical Engineering and Information Systems, Graduate School of Engineering, The University of Tokyo*

## Authors

Wenbo Lin: He studies the control of light based on photonic nanostructures. In this joint study, he was responsible for the device design, fabrication, and optical characterization.

Saeko Tachikawa: She studies the thermal transport in nanostructures. In this joint study, she was responsible for processing the fabricated device using focused ion beam technology and characterizing the device structure.

## Abstract

Vector beams in which polarization is spatially distributed are being discussed for applications in various fields, and the exploration of methods to generate such beams has been actively conducted. The nanophotonic device-based generation of such beams is deemed to greatly expand the range of their applications. Nevertheless, no general method has been established to generate various vector beams using nanophotonic devices. Here we examine nanophotonic structures for controlling polarization states toward the realization of nanophotonic devices that can generate arbitrary vector beams.

## I. Introduction

Vector beams possess spatially variant polarization states in their spatial mode, which are distinguished from conventional scalar beams with spatially uniform polarization states and find applications in optical traps/tweezers [1], laser material processing [2], and classical/quantum optical communications [3,4]. Additionally, some of such beams can be characterized by their spatial polarization distribution by topology, which is of great interest from the viewpoint of the topological properties of light and the interaction with topological quasiparticles in solids [5]. While the generation of such light beams has been widely demonstrated using bulk optical devices such as  $q$ -plates, there is

still a largely unexplored area in the chip-based generation of such beam, although on-chip devices have exceptional advantages in downsizing and integration hence may find many applications in practical use. Therefore, the establishment of a method to generate various types of vector beams by on-chip devices is highly desired to deepen our knowledge of the physical and topological properties of vector beams and to open up new applications.

Generally, a vector beam can be synthesized from multiple scalar beams with different polarizations and spatial phase and/or amplitude distributions. Polarization states and spatial phase distributions are respectively associated with spin angular momenta (SAMs,  $s$ ) and orbital angular momenta (OAMs,  $l$ ) of light hence a vector beam possesses an angular momentum state of hybridized SAMs and OAMs [6]. Accordingly, on-chip generation of vector beams requires control of both  $s$  and  $l$  by photonic nanostructures. The generation of light beams with controlled angular momenta using nanophotonic devices has been studied extensively in recent years, especially with respect to orbital angular momenta, and various generation methods such as the extraction of the angular momentum of the cavity mode by diffraction have been proposed [7]. Meanwhile, attempts to simultaneously control spin angular momentum are as yet limited [8], hence controlling polarization states by nanophotonic devices is a key issue in realizing on-chip generation of various vector beams.

Here we discuss photonic nanostructures that enable light emissions with controlled SAMs and OAMs. The examined structures are based on the ring resonator illustrated in Fig. 1(a). Due to the strong light confinement of the ring cavity, an effective magnetic field for the confined light is induced, which generates a force in a direction dependent on the traveling direction of the light and the handedness of the circular polarization, resulting in a polarization distribution within the transverse-electric (TE) cavity mode [8], as depicted in the right panel of Fig. 1(a). As a consequence of this polarization distribution, lines of localized circular polarization along the ring emerge in the cavity mode, known as chiral (or  $C$ -) lines [9]. This phenomenon is known as the optical spin-orbit interaction. It is expected that, by periodically arranging small scatterers, e.g., small air holes, along a  $C$ -line, the scatterer array acts as a diffraction grating and selectively diffracts the circular polarization corresponding to that of the  $C$ -line [10], as shown in Figs. 1(b) and (c). These structures can also control the orbital angular momentum  $l$  of the diffracted light depending on the number of periods of the grating, and thereby it is expected to be an excellent platform for generating light beams with both controlled  $s$  and  $l$ . We fabricated this structure by electron beam (EB) lithography and dry etching, and demonstrated that the polarization of the diffracted light can indeed be controlled. For revealing the relationship between the sizes of the air holes and the polarization state of the diffracted light, we have evaluated the cross-sectional structure of the fabricated devices by processing them with the focused ion beam (FIB) technique. We also investigated the fabrication of nanophotonic structures using FIB technology as an alternative to lithography technology.

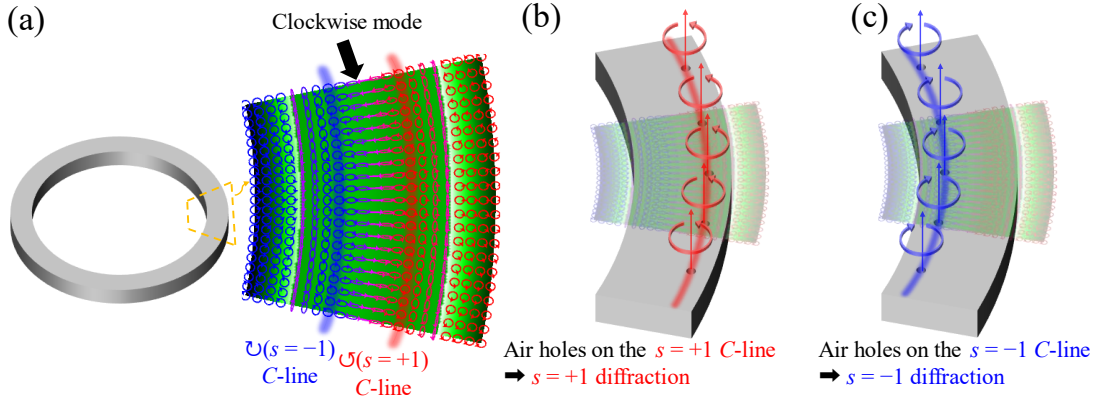


Fig. 1. (a) Schematic of a ring cavity (left panel). The right panel illustrates the intensity and polarization distribution of the fundamental TE-like clockwise cavity mode for the region indicated by the yellow dashed lines in the left panel. The polarization distribution of the cavity mode becomes spatially inhomogeneous due to the optical spin-orbit interaction, which induces the  $C$ -lines of left-handed ( $s = +1$ ) and right-handed ( $s = -1$ ) circular polarizations, which are respectively indicated by the blue line and red line in the right panel. (b) Schematic showing the light diffraction by air holes arranged on the  $s = +1$   $C$ -line. The polarization state of the diffracted light is expected to be  $s = +1$ . (c) Schematic showing the light diffraction by air holes arranged on the  $s = -1$   $C$ -line. The polarization state of the diffracted light is expected to be  $s = -1$ .

## II. Methods

### a. Device fabrication

The examined structure is fabricated by EB lithography and reactive ion etching (RIE). The design pattern is written by dosing EB resist (ZEP520A) spin-coated on a silicon-on-insulator substrate with an electron beam. The designed pattern is formed by immersing the substrate in the developing solution after drawing, which dissolves the resist in the area exposed to the electron beam. The pattern of the resist is transferred onto the silicon by RIE that with  $\text{SF}_6$  gas using the resist as a mask. In the investigated structure, the key point is the diffraction reflects the local polarization of the cavity mode, which is predicted to ideally occur as the size of the air hole decreases. The etching rate of RIE depends on the hole radius, and air holes with smaller radii are expected to have slower etching rates and hence will be shallower.

### b. Device structure evaluation

Since the depth of the air hole is expected to affect the polarization state of the diffracted light, it is important to evaluate the cross-sectional structure of the fabricated device. Although evaluation of device cross-section is often performed by cleavage, the cleavage plane rarely crosses the air hole in the proposed structure because the radius of the air hole is small (typically a few tens of nanometers).

Therefore, the FIB technology is used to machine the silicon and form a cross-section on demand for evaluation. In parallel, we also investigate the potential of FIB technology to fabricate structures with multiple depths, which is not easy to achieve by electron beam lithography and RIE.

### *c. Optical characterization*

The cavity mode of the device is excited by a wavelength-tunable laser, and the diffracted light from the device is evaluated by far-field imaging. The spatial distribution of the polarization in the far field is characterized by filtering the polarization with a quarter-wave plate and a linear polarizer.

## **III. Results and discussions**

### *a. Evaluation of the cross-sectional structure of the fabricated device*

Figure 2(a) shows the top-view scanning electron microscope (SEM) image of one of the fabricated devices. A Si ring resonator and a Si waveguide for optical input were fabricated on SiO<sub>2</sub>. The width of the ring is about 450 nm and the radius is 3  $\mu\text{m}$ . Two arrays of small holes were drilled on the ring to form a double angular diffraction grating. Other devices also were fabricated in which the only one of the two angular gratings was patterned (not shown). Figure 2(b) shows a top-view SEM image of the device with a cross-section formed by FIB to evaluate the cross-sectional structure of the device. Some cross-sections were formed across the air holes so that the depth of the holes on the ring can be observed. Devices with two different air hole radii, 50nm and 30nm, were designed, and Fig. 3(c) shows the enlarged top-view SEM image of a device with a design hole radius of 50 nm. For the device of this design, we accidentally obtained a cross section across the hole by cleavage, and the SEM image of the cleaved surface is shown in Fig. 3(d). The depth of the hole was found to be about 200 nm, which is approximately equal to the height of the ring, 220 nm. Figures 3(e) and (f) show the top SEM image of device with a design hole radius of 30 nm and the SEM image of its cross-section formed by FIB, respectively. It can be seen that the contrast of the cross-section processed by FIB is weaker than that of the cleaved surface by comparing Figs. 3(g) and (f), making it difficult to evaluate the air hole depth accurately. This poor contrast may be due to a combination of factors, including (i) rounded corners of the structure caused by the FIB processing and (ii) charge-up caused by the FIB processing. The depth of the hole was systematically evaluated from multiple device cross-sections and imaging conditions, and was found to be around 110 to 150 nm. Consequently, it was confirmed that devices with a smaller hole radius also had a smaller hole depth.

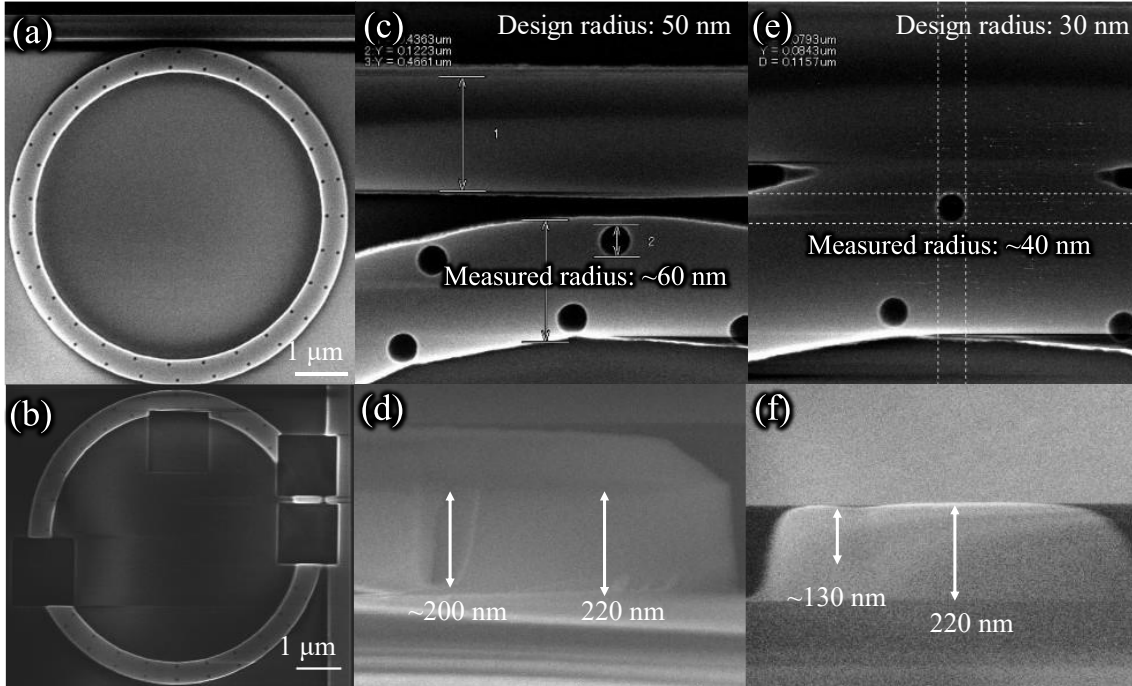


Fig. 2. (a) A top-view SEM image of a fabricated device. (b) A top-view image of a fabricated device with a cross-section processed by FIB. The cross-section is formed across the air holes. (c) A magnified top-view of a device with air holes of a design radius of 50 nm. (d) A cross-sectional view of the structure of (c). This cross section is a cleavage plane, which accidentally crosses an air hole. (e) A magnified top-view of a device with air holes of a design radius of 30 nm. (f) A cross-sectional view of the structure of (e). The cross section is formed by FIB.

### *b. Optical characterization of the fabricated device*

Figure 3(a) shows a schematic of the device designed to diffract left-handed ( $s = +1$ ) circular polarization and the corresponding results of optical measurements and electromagnetic simulations. As shown in Fig. 1, the clockwise resonator mode is locally left-handed circularly polarized near the outer edge of the ring, and thereby the air holes are arranged near the outer diameter of the ring. The device evaluated here is the one with the smaller design hole radius (30 nm). In the experiment, a TE-mode laser was inputted from the left side of the linear waveguide neighboring the ring cavity and evanescently coupled to the cavity to excite the clockwise cavity mode. Here we targeted a cavity mode with a resonance wavelength around 1528 nm. The upper panel on the right side of Fig. 3(a) shows the measured spatial distribution of the Stokes parameters ( $S_0 \sim S_3$ ) in the far field, representing the polarization states. The lower panel of the figure shows the distributions of the far-field Stokes parameters computed by electromagnetic simulation assuming a hole depth of 110 nm, and the results are basically consistent with that of the experiments. The simulation results clearly show that the positive component of  $S_3$  (corresponds to left-handed circular polarization  $s = +1$ ) is dominant, except

in the vicinity of the center, which implies that the expected circularly polarized diffraction is dominant. In the center of the far field, the negative component of  $S_3$  (corresponds to right-handed circular polarization  $s = -1$ ) dominates, which may be due to the slight misarrangement of the air holes from the  $C$ -line of  $s = -1$ . In contrast, the linear polarization components ( $S_1$  and  $S_2$ ) tend to be stronger in the experimental results than that in the simulation results. This is probably due to the reflection of a portion of the input laser that passes through without coupling to the ring, which excites the counterclockwise cavity mode.

Figure 3(b) shows the same set of plots as in Fig. 3(a) for a device designed to diffract right-handed ( $s = -1$ ) circular polarization. In contrast to the device in Figure 3(a), the holes are aligned near the inner diameter of the ring. The polarization measurement shows that the negative component of  $S_3$ , i.e., right-handed circular polarization, is dominant as expected. Similar to the results in Fig. 3(a), the linearly polarized components tend to be stronger in the experimental results than that in the computed results. Figure 3(c) shows the results for a device with the same hole arrangement as the device in Fig. 3(b), but with a larger design value (50 nm) for the hole radius. In the calculation, the depth of the hole is assumed to be 200 nm. In this device, the experimental results and simulation results are not in good agreement. In the simulation results, the negative component of  $S_3$  is dominant, while in the experimental results,  $S_3$  is weak and the linearly polarized component is dominant instead. One possible reason for this unexpected behavior is that the radiation from the ring is stronger due to the larger hole size, which reduces the component of the input laser that couples to the ring, enlarging the effect of the reflections.

The above results show that the experimental and computational results are in good agreement for designs with small air hole radii and depths, and that the circular polarization state of the diffracted light at the far field can be controlled by the radial position of the holes.

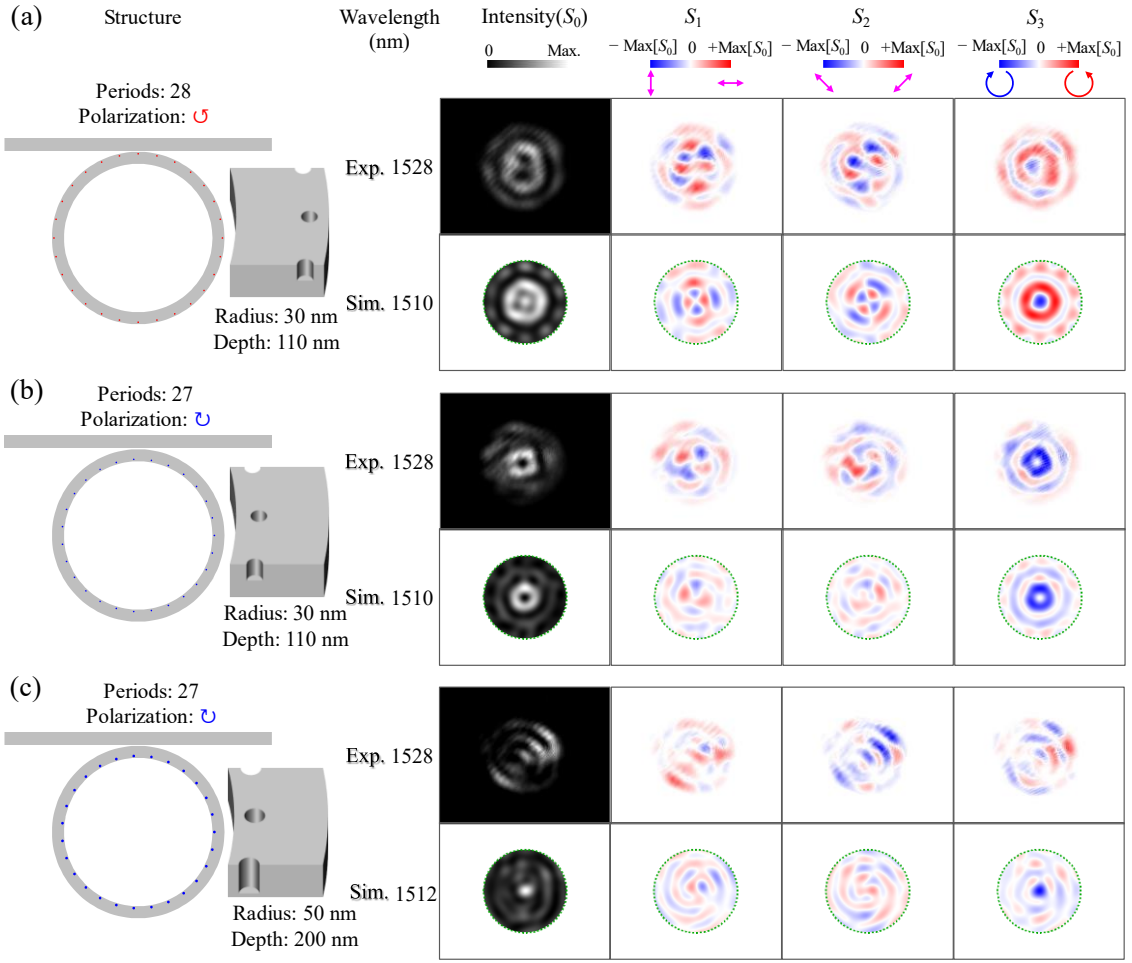


Fig. 3. (a) Schematic of the device with 28 holes of 30 nm radius near the outer edge of the ring (left panel) and the intensity and polarization distributions in the far field (right panel). The top row shows the experimental results, while the bottom row shows the simulation results. This device is expected to diffract left-handed ( $s = +1$ ) circularly polarized light. The hole depth is assumed to be 110 nm in the simulations. (b) The same set of plots as in (a) but for the device with 27 holes of 30 nm radius near the inner edge of the ring. The expected diffraction is right-handed circular polarization ( $s = -1$ ) and the hole depth is assumed to be 110 nm in the simulations. (c) The same set of plots as in (b) but for the device with 27 holes of 50 nm radius near the inner edge of the ring. The expected diffraction is right-handed circular polarization ( $s = -1$ ) and the hole depth is assumed to be 200 nm in the simulations.

### c. Investigation of nanophotonic structure fabrication by focused ion beam technology

In the structure studied in this paper, the degree of circular polarization in diffraction can be further increased by fabricating shallow gratings according to the numerical analysis (not shown). Therefore, it is important to develop a technique to precisely arranging shallower gratings to achieve a more ideal

device operation. Although electron beam lithography is an excellent nanofabrication technique used in the fabrication of the devices in this study, it requires multiple lithography cycles or grayscale lithography to fabricate structures with steps. Fabricating stepped structures with multiple lithography cycles requires alignments thus the alignment errors are unavoidable. The conditions for grayscale lithography are often unstable, hence the development of the process is not easy. Thus, there are many challenges to fabricate shallow gratings on rings by electron beam lithography with high position accuracy. We have therefore investigated the feasibility of fabricating devices using FIB technology instead of electron beam lithography. Since FIB scrapes materials locally and directly by ion irradiation, the depth of processing can be flexibly controlled by the exposure time, enabling simultaneous fabrication of structures of various depths. Figures 4(a)–(c) show the structures made via FIB. Figure 4(a) shows four holes drilled on a single ring resonator with the same exposure time. The contrast of the four holes in the SEM picture is almost the same, indicating that the depth of the holes is roughly the same. In contrast to this condition, Fig. 4(b) shows four holes processed on a single ring cavity while changing the processing time. The contrast is different for each hole, indicating that holes with different depths are formed. Figure 4(c) shows the result of punching holes not on the Si ring but in the SiO<sub>2</sub> layer on which the ring is mounted. This is also a structure that is difficult to fabricate by lithography technology. These investigations suggest that FIB can be used to fabricate devices with high flexibility. In this trial, the shapes that could be processed were limited to the primitives of the FIB system because they were drawn manually. However, arbitrary shapes can be processed by creating patterns in advance, and it is expected that arbitrary optical devices can be fabricated by FIB machining. Optical characterization of the fabricated device was also conducted, but the signal from the ring was weak probably due to the small number of holes, and we could not obtain clear measurement results.

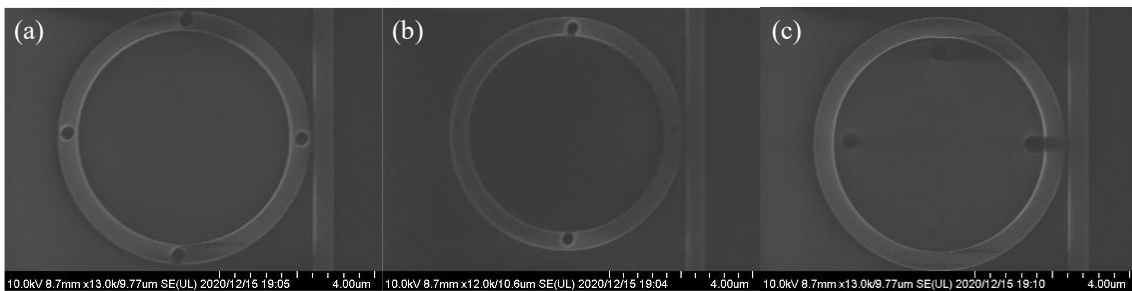


Fig. 4. Microstructures fabricated by the FIB machining. (a) Top-view SEM image of four holes that are machined on a silicon ring under the condition that the processing time is the same for all four holes. (b) The same as (a) but for the condition that the processing time was modulated. The depths of the holes are different. (c) Top-view picture of four holes that are machined on the SiO<sub>2</sub> layer.

#### IV. Summary and Prospects

In summary, we evaluated a structure with a diffraction grating along the ring cavity and demonstrated

that the structure enables light diffraction with a controlled state of polarization. We also revealed that the diffraction grating works ideally when the size of scatterers constituting the grating is small. By using this structure, both right-handed and left-handed circular polarizations can be emitted from the ring resonator. The right-handed circular polarization and the left-handed circular polarization are two orthogonal polarization states, and an arbitrary polarization state can be obtained by superposing them. Therefore, it is expected that two circularly polarized beams can be diffracted simultaneously by patterning two diffraction gratings on the same ring, as shown in Fig. 2(a), and a variety of polarization distributions can be obtained as a superposition of the two beams. Indeed, we have observed that an optical beam with a unique polarization distribution, such as a skyrmion, can be generated by a ring resonator with a double grating (not shown). A shallower grating would bring the structure closer to the ideal behavior, and therefore, developing a technique to fabricate a shallower grating is important. We have verified that the processing depth can be closely controlled by the FIB technique, thereby this technique is a promising candidate for fabricating shallow gratings.

## Acknowledgements

The authors appreciate Prof. Iwamoto and Prof. Nomura for their thoughtful support and insightful advice. The authors are grateful to Prof. Katsumoto and the MERIT program for giving us this precious opportunity for this joint research.

## References

- [1] S. E. Skelton, M. Sergides, R. Saija, M. A. Iati, O. M. Maragó, and P. H. Jones, “Trapping volume control in optical tweezers using cylindrical vector beams”, *Optics Letters* **38**, 28 (2013).
- [2] M. Kraus, M. A. Ahmed, A. Michalowski, A. Voss, R. Weber, and T. Graf, “Microdrilling in steel using ultrashort pulsed laser beams with radial and azimuthal polarization”, *Optics Express* **18**, 22305 (2010).
- [3] G. Milione, M. P. J. Lavery, H. Huang, Y. Ren, G. Xie, T. A. Nguyen, E. Karimi, L. Marrucci, D. A. Nolan, R. R. Alfano, and A. E. Willner, “ $4 \times 20$  Gbit/s mode division multiplexing over free space using vector modes and a q-plate mode (de)multiplexer”, *Optics Letters* **40**, 1980 (2015).
- [4] V. D’Ambrosio, E. Nagali, S. P. Walborn, L. Aolita, S. Slussarenko, L. Marrucci, and F. Sciarrino, “Complete experimental toolbox for alignment-free quantum communication”, *Nature Communications* **3**, 961 (2012).
- [5] S. Donati, L. Dominici, G. Dagvadorj, D. Ballarini, M. De Giorgi, A. Bramati, G. Gigli, Y. G. Rubo, M. H. Szymańska, and D. Sanvitto, “Twist of generalized skyrmions and spin vortices in a polariton superfluid”, *Proceedings of the National Academy of Sciences* **113**, 14926 (2016).
- [6] S. Chen, X. Zhou, Y. Liu, X. Ling, H. Luo, and S. Wen, “Generation of arbitrary cylindrical vector beams on the higher order poincaré sphere”, *Optics Letters* **39**, 5274 (2014).

- [7] X. Cai, J. Wang, M. J. Strain, B. Johnson-Morris, J. Zhu, M. Sorel, J. L. O'Brien, M. G. Thompson, and S. Yu, "Integrated compact optical vortex beam emitters", *Science* **338**, 363 (2012).
- [8] Z. Shao, J. Zhu, Y. Chen, Y. Zhang, and S. Yu, "Spin-orbit interaction of light induced by transverse spin angular momentum engineering", *Nature Communications* **9**, 926 (2018).
- [9] R. J. Coles, D. M. Price, J. E. Dixon, B. Royall, E. Clarke, P. Kok, M. S. Skolnick, A. M. Fox, and M. N. Makhonin, "Chirality of nanophotonic waveguide with embedded quantum emitter for unidirectional spin transfer", *Nature Communications* **7**, 11183 (2016).
- [10] W. Lin, Y. Ota, Y. Arakawa, and S. Iwamoto, "Microcavity-based Generation of full poincaré beams with arbitrary skyrmion numbers," arXiv:1906.05333 (2020).